Design of, and Initial Experiments with, a MIMO Plate Control Testbed

by

Daniel G. Cole

Thesis submitted to the Faculty of the

Virginia Polytechnic Institute and State University

in partial fulfillment of the requirements for the degree of

Master of Science

in

Mechanical Engineering

APPROVED:

H. H. Robertshaw

Prof. H. H. Robertshaw, Chairman

W. T. Baumann

Prof. W. T. Baumann

Harley H Cudney

Prof. H. H. Cudney

September 1, 1992
Blacksburg, Virginia

Design of, and Initial Experiments with, a MIMO Plate Control Testbed

by

Daniel G. Cole

Committee Chairman: Harry H. Robertshaw

Mechanical Engineering

(ABSTRACT)

This work discusses the design of, and initial experiments with, a MIMO plate control testbed. This structure will be used as a development and standard comparison site for AVC and ASAC and is an extension of previous SIMO control investigations which used accelerometers and shakers. This portion of the development process of the MIMO plate control testbed is concerned with actuator and sensor materials and architecture, modeling approaches and requirements, and initial control experiments.

The piezoelectric sensors and actuators are arranged on the plate to control the first five vibration modes. The sensors measure plate positions using a high impedance signal conditioning amplifier. The sixteen-channel design implements a band-pass filter to eliminate low- and high-frequency noise.

The power amplification scheme chosen for the actuators uses low-gain amplifiers ($\sim$2.5 V/V) in series with a transformer (24:1) to deliver high voltages (up to 150 V) to the actuators. Low-pass smoothing filters (200 Hz cutoff) were added on the control inputs to reduce the high frequency content of the zero-order-held digital control signal.

Initial methods for system identification of piezostructures are presented. Parametric frequency response approaches (modal analysis) were used and the model achieved is compared with measured data and purely analytic models.

The empirical model was used in initial SIMO control experiments to demonstrate the testbed closed-loop performance. A LQG controller was implemented and produced 6 dB of suppression for the second mode for a 110 Hz disturbance.

Acknowledgements

I would like to thank those people who helped me through this project. First, thanks should go to Harry Robertshaw without who's advice and support I might have given up in the beginning. Thanks to my other committee members Dr. Baumann and Dr. Cudney for their advise and suggestions.

Thanks to Will Saunders for working with me through the long haul and teaching me the thing I really needed to know to make things work. There is no doubt in my mind that this project would have gone nowhere without his help. Thanks also to the others in the lab whose help and humor will be remembered: Buddy Clark, Ken Ellis, Gary Fagan, Robert Wynn, etc.

Lastly I want to thank my family for instilling in me the curiosity to continue my education. Thank you Dad, David, Charlie, Connie, Tom, Jim, and Mary. Most of all thank you Mom for sticking with me. This one's for you.

Contents

List of Figures

List of Tables

List of Symbols

a	plate length — x direction	m
	transformer turns ratio	—
b	plate length — y direction	m
c	stiffness matrix (Hooke's law)	N/m^2
d	piezoelectric constant (strain/field)	m/V
e	piezoelectric constant (stress/field)	$N/V \cdot m$
f	force	N
	frequency	Hz
h	plate half thickness	m
k	wave number	m^{-1}
nf, nq	number of forces, electrodes	—
q	charge	C
	modal coordinate	$kg^{1/2} \cdot m$
r	generalized coordinate	
s	Laplace variable	s^{-1}
t_p	piezoelectric thickness	m
u	displacement	m
v	generalized voltage	
w_x, w_y	piezoelectric width	m
x	position	m
A_i	area i^{th} patch	m^2
A^r_{ij}	residues	
B_f	mechanical forcing matrix	—
B_q	electrical forcing matrix	—
C	damping matrix	$N \cdot s/m$
	capacitance	C
	output matrix	
C_p	capacitance matrix	C
D	electric displacement	$C \cdot m$
E	electric field	V/m

K	stiffness matrix	N/m
	amplifier gain	—
	feedback gain matrix	
K_f	Kalman filter gain matrix	
L_u	strain-displacement differential operator	m^{-1}
L_φ	field-voltage differential operator	m^{-1}
M	mass matrix	kg
R	resistance	Ω
S	strain	—
S_j	first area moment	m
T	stress	N/m^2
U_{ke}	kinetic energy (mechanical)	J
U_{pe}	potential energy (mechanical)	J
V	voltage	V
V_s, V_p	volume of structure, piezoelectric	m^3
W	work	J
W_e	energy (electrical)	J
W_m	energy (magnetic)	J
ε	material permittivity	$C^2/N \cdot m^2$
ε_0	permittivity of free space	$C^2/N \cdot m^2$
ζ	damping coefficient	—
λ	wavelength	m
ρ	density	kg/m^3
φ	voltage	V
ω	frequency	rad
Γ	discrete input matrix	
Θ	electromechanical coupling matrix	N/V
Φ	eigenvector matrix	$kg^{-1/2}$
	discrete dynamics matrix	—
Ψ_r	displacement mode	
Ψ_φ	voltage mode	
$()^T$	transpose	
$()_a$	actuator	
$()_s$	sensor	
$()_E$	constant electric field	
$()_S$	constant strain	
$()_T$	constant stress	

Chapter 1

Introduction

Recent research efforts have been focused on design and control of intelligent structures. Intelligent structures are characterized by sensors and actuators which can be networked through a control system to produce robust control which can withstand or adapt to variations in controlled plant responses, environmental disturbances, and control system failures. Such an approach would allow the use of flexible control strategies to tune the response of the structure for different control approaches and performance measures.

Of primary importance to such a control system design approach are actuators and sensors. Since there are typically a large number of inputs and outputs it is beneficial and desirable to have compact sensors and actuators which are simple to use and do not greatly affect the open-loop response of a structure. Recent studies have shown piezoelectric materials are effective compact actuators and sensors.

A majority of the vibration control research published to date has been concerned with beams and low-order controllers (SISO & SIMO) which drastically limit controller performance. Most MIMO control studies have investigated decentralized control. In addition, few experimental studies have approached MIMO control using digital control paradigms.

This work discusses the design of, and initial experiments with, a MIMO plate control testbed. A simply-supported plate was chosen as the testbed structure for medium complexity and well defined behavior. This structure will be used as a development and standard comparison site for Active Vibration Control (AVC) and Active Structural Acoustic Control (ASAC) and is an extension of previous single-input/multi-output (SIMO) control investigations which used more proven technology (accelerometers and shakers). This portion of the design process for a MIMO plate control testbed develops actuator and sensor materials and architecture, modeling approaches and requirements, and initial control experiments.

The sixteen piezoelectric sensors and five piezoelectric actuators, chosen for both their size and effectiveness, are arranged on the plate to control the first five vibration modes. At present the controller software is limited to a sample speeds of ~2000 Hz. For the simply-supported testbed this limits control to the first five modes (less than 200 Hz). The sensors have been configured to measure plate positions necessitating the design of signal conditioning amplifiers due to the sensors low voltage output and high impedance (80 MΩ) within the operating frequency range. The term *position* refers to plate positions in general, while specific types of positions will be expressly stated, e.g. modal positions. The resulting sixteen channel custom design implements a band-pass filter to eliminate low frequency variations and high frequency noise using a two stage operational amplifier (op-amp) configuration.

Various actuator power amplification methods for the actuators were considered, among them high voltage analog amplifiers and pulse-width modulation. The voltage amplification scheme chosen uses low gain amplifiers (~2.5 V/V) in series with a transformer (24:1) to deliver the relatively high voltages (up to 150 V) to the actuators. This avenue was chosen over more elegant and expensive methods because its

dynamics could be easily modeled and included in the mathematical models required to generate control laws. In addition, the amplifier-transformer pairs could be constructed with relative ease and short lead time. Low-pass smoothing filters (200 Hz cutoff) were added to reduce the high frequency content of the zero-order-held control signal coming from the computer and are also included in the system models.

Analytical models, which offer insight and perception into system behavior, are typically not accurate enough for to control law calculation of real systems. Experimentally determined models have proven to be more reliable and are preferred in the computation of control algorithms. The identification of piezostructures is complicated since forces applied to the structure are unmeasurable and quantifying the electromechanical coupling provided by piezoelectrics is difficult. Initial methods for system identification of piezostructures are presented. Parametric frequency response approaches (modal analysis) were used and the model achieved is compared with measured data and pure analytic models.

Lastly, the empirical model was used to design a controller in initial SIMO control experiments to demonstrate the testbed closed-loop performance. A LQG controller, which combines LQR feedback control with an optimal stochastic estimator (Kalman filter), was implemented as the control algorithm and produced 6 dB of suppression for the second mode while the structure was excited by a 110 Hz disturbance near the second mode resonant frequency. While these experiments did demonstrate the testbed under control, more system identification work is required.

Chapter 2

Literature Review

Piezoelectric materials, which produce a voltage due to strains in a crystal under the direct piezoelectric effect and change shape by the application of a voltage under the converse piezoelectric effect, were discovered by the Curie brothers in the late nineteenth century. Not much progress was made toward applications of the new phenomenon during the first third of a century since its discovery. The advent of World War I found applications of piezoelectric crystals as high frequency acoustic transducers. Since that time piezoelectrics have found a wide range of applications from accelerometers to highly constant time standards (Mason 1981). Most recently there has been a push to explore the use of piezoelectrics as both actuators and sensors in the implementation and control of intelligent structures.

Swigert & Forward (1981) performed one of the first studies of piezoelectrics in intelligent structures. They used piezoelectrics as both strain sensors and strain 'drivers' in an experiment to add electronic damping to bending modes of a cylindrical mast. They showed through numerical and physical experiments that moderate levels of damping could be achieved in the first two bending modes at low feedback gains. Higher levels of damping were achieved for greater feedback gains and for an increased number of orthogonal electronic damping circuits. However, their investigation did

not model the piezoelectric/structure interaction.

In 1985, Bailey & Hubbard (1985) developed a model of piezoelectric actuators and showed that the effective force of a piezoelectric actuator is proportional to the voltage and that this constant can be determined from material and structural properties. They used their model to design an active vibration damper for a cantilevered beam with favorable results.

Crawley & de Luis (1987) further extended Bailey & Hubbard's (1985) work into more comprehensive analytic models of piezoelectrics as actuators. They developed both pure bending and pure extensional models of piezoelectrics as embedded and surface bonded actuators. They showed that actuator effectiveness not only depends on material properties but also on actuator location and size. A scaling analysis was done to demonstrate that the effectiveness of piezoelectric actuators is independent of the size of the structure. Experimental results compared well with those found using the analytical model. Since their research, numerous models of fundamentally similar derivation have been presented (Crawley & Anderson 1989; Crawley & Lazarus 1989; Dimitriadis et al. 1991; Im & Atluri 1989; Pan et al. 1991; Tzou 1992; Wang & Rogers 1990, 1991). These models have been experimentally verified in de Luis & Crawley (1990), Clark et al. (1991) and Flemming (1990).

While these models apply to various one and two dimensional structures (beams and plates) with different assumed thickness strain distributions, all have been derived using a Newtonian approach. This method considers stress/strain distributions, the shear force applied between the piezoelectric/structure interface and the induced strain of the piezoelectric to calculate an applied moment which is proportional to the applied voltage as mentioned before. This applied moment is shown to act along lines at the edges of a piezoelectric actuator patch.

It is typically assumed in models developed using the Newtonian approach that the added mass and stiffness of piezoelectrics are small and that the actuator will act quasistatically compared to the structure (Crawley & de Luis 1987). Thus, the analysis of the applied forces is done with static considerations and then incorporated into a larger dynamic model. This may or may not be a good assumption, depending upon the relationship between structure mass and stiffness and that added by the piezoelectrics.

When the applied line moment is used in the equation of motion for the structure the analysis typically leads to a modal representation of the system. In this case the modal force depends both on the magnitude of the applied moment and the slope of the structure at the edges of the patch. Typical representations of the modal force are a function of the applied moment and the difference in the slope from one edge of an actuator to the other. It is often difficult to determine the modal rotation eigenvectors experimentally for physical structures, thereby restricting the usefulness of this approach. Also, the static models do not account for the charge generated by a piezoelectric patch. The dynamics associated with the movement of this charge to and from the electrodes of a piezoelectric can be quite useful, especially when designing passive damping circuits (Cudney 1989; Hagood & Crawley 1989; Hagood & von Flotow 1989).

Hagood et al. (1990) used energy methods to develop a model that considered both the coupled dynamics between the structure and piezoelectric sensor/actuators and electrodynamics of the piezoelectrics. Mechanical energy terms (kinetic and potential) were found for both the structure and piezoelectrics. In addition, the energy stored in electric fields was included. Introducing constitutive equations and applying variations to Hamilton's principle, they arrived at two equations which describe the

electromechanical interaction of the piezoelectric/structure system.

$$\begin{aligned} M\ddot{r} + C\dot{r} + Kr &= B_f f + \Theta v \\ \Theta^T r + C_p v &= B_q q \end{aligned}$$

where M, C, K are mass damping and stiffness matrices respectively, Θ is the electromechanical coupling matrix, C_p is the piezoelectric capacitance matrix, B_f, B_q are the mechanical and electrical forcing matrices and r, v, q, f are the generalized coordinate, piezoelectric voltage, piezoelectric charge and applied point forces respectively. A derivation following Hagood et al. (1990) is included in Chapter 3. Similar derivations have been shown in Burke & Hubbard (1991), Tzou & Gadre (1989), and Tzou & Tseng (1990a, 1990b). The above equations are easily incorporated into state space equations and will be used throughout this work. The majority of the investigations mentioned have been concerned with controlling simple one-dimensional beams. The model developed by Hagood et al. (1990) adapts well to multi-dimensional structures.

As previously stated the main thrust of recent piezoelectric research has been to investigate uses in intelligent structures. Through the use of programmable control algorithms structural responses can be tuned as desired. One major area of interest is the control of structural vibrations and structural acoustics, both transient and steady state.

The majority of investigations into intelligent structure implementation of piezoelectrics has been with rate feedback control algorithms (Bailey & Hubbard 1985; Chaing & Lee 1989; Crawley & de Luis 1987; Hanagud et al. 1988; Lee et al. 1989, 1991; Sung et al. 1990; Swigert & Forward 1981; Tzou 1992; Tzou & Gadre 1989; Tzou & Tseng 1990a, 1990b). Rate feedback schemes investigated include proportional feedback and constant amplitude feedback. These control laws have the benefit of only adding damping thus guaranteeing stability. The ability of piezoelectric to add

damping is promising, also indicating that inclusion into more complicated control laws could be done. Piezoelectrics are attractive to rate feedback algorithms since, if their signal is properly conditioned, a strain rate signal can be obtained (Lee & O'Sullivan 1991).

The LMS algorithm has also been used with piezoelectrics as a means of reducing the effects of persistent disturbance (Gibbs & Fuller 1990; Clark & Fuller 1991). A Filtered-X version of the LMS algorithm was used with multiple sensors and actuators (Clark & Fuller 1990). In principle this method has the benefit of not having to explicitly model the piezoelectric/structure interaction. However, work done by the preceding authors has included numerical simulations which compared well with experimental results and used previous theories.

The Modified Independent Modal Space (MIMSC) control algorithm has been studied with piezoelectrics as sensors and actuators (Baz & Poh 1987, 1988, 1990). The method minimizes the vibrations in a beam as well as the control effort needed to control vibrations. The method also accounts for the effect that piezoelectrics and bonding layers have on the elastic and inertial properties of a structure. The MIMSC algorithm relies on one actuator to control multiple modes of vibration by using a unique time sharing algorithm.

Hanagud et al. (1987) investigated optimal vibration control using a quadratic cost functional. They used output feedback rather than full-state feedback in their control law and calculated feedback gains using a solution procedure outlined in Moerder & Calise (1985). A function of the control gains was added to the cost functional to ensure a diagonal gain matrix and collocated control. Only numerical experiments were performed for control of a cantilevered beam. While their collocated output feedback method had favorable results, they observed that systems with cross

feedback terms have better performance.

De Luis & Crawley (1990) also investigated optimal vibration control minimizing a quadratic cost functional. Velocity and curvature were selected as states. This selection of states resulted in the the optimal control at a particular actuator location (for a diagonal Q and R) is a function of the collocated velocity and collocated curvature. This result is particular to the choice of states and induced strain actuators, i.e. piezoelectric actuators. This formulation allows highly decentralized controllers to be designed without an increase in the performance cost functional. De Luis and Crawley performed MIMO control experiments on a cantilevered beam with satisfactory results.

Both of these studies pursued optimal controls using collocated feedback. Implementation of the control scheme was accomplished using analog amplifiers. Drawbacks to the schemes are that they provide little ability to change and adapt to account for unmodeled dynamics, changing design criteria (acoustic v. vibration control), and the existence of persistent disturbances. They also limit the controller authority by only allowing collocated feedback. A digital realization of the control schemes would allow for more flexibility in altering the controller to produce the desired closed loop characteristics and also allow for easy implementation of disturbance rejection methods and adaptive schemes.

A study conducted by Rubenstein (1991) investigated state-space vibration control of steady disturbances on a simply supported plate. This research implemented an LQG/Kalman filter state feedback approach to cancel persistent disturbances. The experiment was single-input/multi-output (SIMO) using shakers for disturbance and control forces and accelerometers as sensors. Rubenstein demonstrated control of vibrations caused by both harmonic and narrowband disturbances close to first mode

resonance.

Rubenstein's work used proven technology in shakers and accelerometers to design a SIMO plate control testbed. Modal properties of light structures can be drastically changed by adding comparatively heavy actuators and sensors. Also, actuators such as shakers are bulky and difficult to implement on many real world structures. MIMO control strategies, using shakers, would be impractical considering their size and weight and even relatively light accelerometers alter passive eigenproperties drastically thus confusing the designed simplicity of a simply supported plate testbed. Piezoelectrics are small and light weight and offer promise as actuators in intelligent structures (Crawley and de Luis 1987).

The work reported here discusses the design of a MIMO plate control testbed which takes advantage of light, compact piezoelectric sensors and actuators. Modeling issues associated with incorporating piezoelectrics in a structural model and using them as actuators and sensors will be discussed first. Since piezoelectrics couple electrical and mechanical systems a discussion of the electrical circuitry designed for the experimental test bed will be considered. System identification techniques and initial results will also be explained. Finally initial experimental results using piezoelectrics in an LQG control scheme will be shown.

Chapter 3

Modeling

In order to design an Active Vibration Controller (AVC) or Active Structural Acoustic Controller (ASAC) the electromechanical interaction offered by the piezoelectrics must be modeled. While this is a prerequisite for controller design, it will also allow for performance prediction and parametric studies to optimize characteristics such as size, location, and thickness. The method used to characterize the piezo/structure interaction follows the method outlined in Hagood et al. (1990). The plant controlled in the experimental work is a simply-supported plate. The selection and design of a simply-supported plate is discussed in Rubenstein (1991). This chapter discusses the Hagood model and its application to a simply-supported plate and the issues associated with using piezoelectrics as sensors and actuators.

3.1 General model

This section discusses the modeling method developed in Hagood et. al. (1990). This method uses an energy approach to find the equations of motion and will be repeated here. It accounts for the mass and stiffness loading of the piezoelectrics as well as the electrodynamics associated with coupling the piezostructure to electronics.

From Hamilton's principle for coupled electromechanical systems (Crandall et al.

1968):

$$\int_{t_1}^{t_2}[\delta(U_{ke} - U_{pe} + W_e - W_m) + \delta W]dt = 0 \tag{3.1}$$

for piezoelectrics the magnetic term, W_m, is negligible. The other terms are defined as follows.

$$U_{ke} = \int_{V_s} \frac{1}{2}\rho_s \dot{u}^T \dot{u} + \int_{V_p} \frac{1}{2}\rho_p \dot{u}^T \dot{u} \tag{3.2}$$

$$U_{pe} = \int_{V_s} \frac{1}{2} S^T T + \int_{V_p} \frac{1}{2} S^T T \tag{3.3}$$

$$W_e = \int_{V_p} \frac{1}{2} E^T D \tag{3.4}$$

If we consider only discrete point forces and a finite number of piezoelectric electrodes then,

$$\delta W = \sum_{i=1}^{nf} \delta u(x_i) \cdot f(x_i) - \sum_{j=1}^{nq} \delta\varphi_j \cdot q_j \tag{3.5}$$

introducing constitutive equations for the structure material,

$$T = cS \tag{3.6}$$

and the piezoelectrics,

$$D = \varepsilon_S E + eS \tag{3.7}$$

$$T = -e^T E + c_E S \tag{3.8}$$

where in the above relationships

$$e = dc_E \tag{3.9}$$

$$\varepsilon_S = \varepsilon_T - dc_E d^T \tag{3.10}$$

From the theory of elasticity a strain-displacement relationship can be introduced.

$$S = L_u u(x) \tag{3.11}$$

where L_u is the linear differential operator specific to the problem being solved. Also the field-potential (field-voltage) relationship is

$$E = L_\varphi \varphi(x) = -\nabla \cdot \varphi(x, y, z) \tag{3.12}$$

here L_φ is the gradient operator.

The displacement at position x can be represented in terms of the generalized coordinates.

$$u(x,t) = \Psi_r(x) r(t) = [\Psi_{r_1}(x) \cdots \Psi_{r_n}(x)] \begin{bmatrix} r_1(t) \\ \vdots \\ r_n(t) \end{bmatrix} \tag{3.13}$$

Here the assumed displacement distributions, i.e. mode shapes, only have to satisfy the geometric boundary conditions.

A similar approach is taken with the electric potential (voltage):

$$\varphi(x,t) = \Psi_v(x) v(t) = [\Psi_{v_1}(x) \cdots \Psi_{v_m}(x)] \begin{bmatrix} v_1(t) \\ \vdots \\ v_n(t) \end{bmatrix} \tag{3.14}$$

Here it will be convenient to have the v_i represent the physical voltages of the electrodes.

The equations of motion can be derived by substituting equations 3.2–3.8 into Hamilton's equation (3.1) and taking variations:

$$\begin{aligned} \int_{t_1}^{t_2} \Bigg[\int_{V_s} \rho_s \delta \dot{u}^T \dot{u} + \int_{V_p} \rho_p \delta \dot{u}^T \dot{u} - \int_{V_s} \delta S^T c_s S - \int_{V_p} \delta S^T c_E S \\ + \int_{V_p} \delta S^T e^T E + \int_{V_p} \delta E^T e S + \int_{V_p} \delta E^T \varepsilon_S E \\ + \sum_{i=1}^{nf} \delta u(x_i) \cdot f(x_i) - \sum_{j=1}^{nq} \delta \varphi_j \cdot q_j \Bigg] dt \;=\; 0 \end{aligned} \tag{3.15}$$

The first two terms in equation 3.15 can be integrated by parts with respect to time and then substitute in equations 3.11–3.14. Allowing for arbitrary variations in

r and v two matrix equations in the generalized coordinates are found.

$$\text{Actuator Eqn.} \qquad M\ddot{r} + K\dot{r} = B_f f + \Theta v \tag{3.16}$$

$$\text{Sensor Eqn.} \qquad \Theta^T r + C_p v = B_q q \tag{3.17}$$

These are the so called actuator and sensor equations, respectively. The coefficient matrices are defined as follows:

$$M = \int_{V_s} \Psi_r^T \rho_s \Psi_r + \int_{V_p} \Psi_r^T \rho_p \Psi_r \tag{3.18}$$

$$K = \int_{V_s} \Psi_r^T L_u^T c_s L_u \Psi_r + \int_{V_p} \Psi_r^T L_u^T c_E L_u \Psi_r \tag{3.19}$$

$$C_p = \int_{V_p} \Psi_v^T L_\varphi^T \varepsilon_S L_\varphi \Psi_v \tag{3.20}$$

$$\Theta = \int_{V_p} \Psi_r^T L_u^T e^T L_\varphi \Psi_v \tag{3.21}$$

$$B_{f_{ij}} = \Psi_{r_i}^T(x_{f_j}) \tag{3.22}$$

$$B_{q_{ij}} = \Psi_{v_i}(x_{q_j}) \tag{3.23}$$

3.2 Simply Supported Plate

The general equations for a piezoelectrically coupled electromechanical system will be applied to an ideal simply supported plate. A Bernoulli-Euler plate model will be assumed. The emphasis here will be on the matrices which characterize the electromechanics, Θ, C_p and B_q.

Structural mode shapes are assumed now. It is possible to determine the electromechanical coupling matrix Θ and the capacitance matrix C_p experimentally thus having a more accurate model of the system. This will be explained in more detail later. For our purposes we will complete this analysis with ideal simply-supported plate mode shapes. The solution of the two-dimensional wave equation with simply-

supported boundary conditions yields mode shapes,

$$\Psi_{ri}(x,y) = \sin(k_{xi}x)\sin(k_{yi}y) \tag{3.24}$$

$$k_{xi} = \frac{m_i\pi}{a} \tag{3.25}$$

$$k_{yi} = \frac{n_i\pi}{b} \tag{3.26}$$

and the first five modes are ordered as follows.

i	m_i	n_i
1	1	1
2	2	1
3	1	2
4	2	2
5	3	1

(3.27)

Using these modes and assuming the displacements are separable in space and time the transverse displacements can be represented as,

$$u(x,y) = [\Psi_{r1}(x,y)\cdots\Psi_{rn}(x,y)]\begin{bmatrix} r_1(t) \\ \vdots \\ r_n(t) \end{bmatrix} \tag{3.28}$$

The strain field under Bernoulli-Euler assumptions is,

$$S = L_u u(x,y) = \begin{bmatrix} -z\partial^2/\partial x^2 \\ -z\partial^2/\partial y^2 \\ -z\partial^2/\partial x\partial y \end{bmatrix} u(x,y) \tag{3.29}$$

The electric field can be represented similarly as

$$E(x,y) = L_\varphi\varphi(x,y,z) = \left[-\frac{\partial}{\partial z}\right]\varphi(x,y,z) \tag{3.30}$$

$$\varphi(x,y,z) = [\Psi_{v1}(x,y,z)\cdots\Psi_{vn}(x,y,z)]\begin{bmatrix} v_1(t) \\ \vdots \\ v_n(t) \end{bmatrix} \tag{3.31}$$

The voltage modes are assumed to vary linearly through the thickness of each piezoelectric.

$$\Psi_{vi} = \begin{cases} \frac{z-h}{t_{pi}} & x_{1i} \le x \le x_{2i} \quad y_{1i} \le y \le y_{2i} \\ 0 & \text{elsewhere} \end{cases} \tag{3.32}$$

Applying the gradient operator to the voltage yields a field proportional to the voltage applied to the electrode.

$$E(x,y) = \begin{cases} -\frac{1}{t_{p_i}} v_i & x_{1i} \leq x \leq x_{2i} \quad y_{1i} \leq y \leq y_{2i} \\ 0 & \text{elsewhere} \end{cases} \tag{3.33}$$

The materials constants e and ε_S are

$$e = \begin{bmatrix} e_{31} & e_{32} & 0 \end{bmatrix}^T \tag{3.34}$$

$$\varepsilon_S = \varepsilon_3 \tag{3.35}$$

The electromechanical matrices are now represented as integral functions over the area and thickness of the j^{th} piezoelectric. Substituting equations 3.28, 3.29 and 3.34 into equation 3.21 yields

$$\theta_{ij} = S_j \int_{x_{1j}}^{x_{2j}} \int_{y_{1j}}^{y_{2j}} \left(e_{31,j} \frac{\partial^2 \Psi_{ri}}{\partial x^2} + e_{32,j} \frac{\partial^2 \Psi_{ri}}{\partial y^2} \right) dy dx \tag{3.36}$$

The first area moment S_j is defined to be

$$S_j = \frac{1}{t_{p_j}} \int_h^{h+t_{p_j}} z dz \tag{3.37}$$

using the ideal simply supported mode shapes gives

$$\theta_{ij} = -S_j \left(\frac{e_{31,j} k_{x_i}^2 + e_{32,j} k_{y_i}^2}{k_{x_i} k_{y_i}} \right) \cos k_{x_i} x \Big|_{x_{1j}}^{x_{2j}} \cos k_{y_i} y \Big|_{y_{1j}}^{y_{2j}} \tag{3.38}$$

The cosine terms can be further simplified to give

$$\theta_{ij} = -S_j \left(\frac{e_{31,j} k_{x_i}^2 + e_{32,j} k_{y_i}^2}{k_{x_i} k_{y_i}} \right) 4 \sin k_{x_i} x_{0j} \sin k_{y_i} y_{0j} \sin k_{x_i} \frac{w_{xj}}{2} \sin k_{y_i} \frac{w_{yj}}{2} \tag{3.39}$$

where (x_0, y_0) is the center of the piezoelectric and w_x and w_y are the widths of the piezoelectric in the x and y directions.

The actuators and sensors used on the MIMO plate testbed are small compared to modal wave lengths for the first five modes. The actuators are (30.48×25.40) mm

and the sensors are (25.40×27.94) mm. Equation 3.39 shows that the effectiveness of the piezoelectrics should increase as the wave number increases (provided $kw < \frac{\pi}{2}$). In addition the expression

$$\frac{e_{31,j}k_{x_i}^2 + e_{32,j}k_{y_i}^2}{k_{x_i}k_{y_i}} \tag{3.40}$$

changes with each mode. It is important to realize that a piezoelectric is more effective on the higher modes. The response of a piezoelectric to the lower modes could be improved by covering more area of the plate, but while this will help the response to the lower modes it introduces spatial aliasing.

In order to maximize a piezoelectric's effectiveness for a particular mode, given the piezoelectrics size, the center location of the piezoelectric should be chosen such that

$$x_0 = \frac{\pi}{2k_x} = \frac{\lambda_x}{4} \tag{3.41}$$

$$y_0 = \frac{\pi}{2k_y} = \frac{\lambda_y}{4} \tag{3.42}$$

that is, placed on an antinode for the mode. Table 3.2 lists the actuator locations and table 3.2 lists the sensor locations. The actuators were placed in the antinodes of the first five modes.

Solution for the capacitance matrix C_p yields a diagonal matrix with entries

$$C_{p_i} = \frac{\varepsilon_i \varepsilon_0 A_i}{t_{p_i}} \tag{3.43}$$

The charge matrix B_q is the identity matrix since the generalized voltages were defined to be the physical electrode voltages. Since the capacitance matrix is diagonal the voltage and charge in the sensor equation are uncoupled electrically and a linear combination of the modal positions.

$$\Theta_i^T r + C_{p_i} v_i = q_i \tag{3.44}$$

Table 3.1: Actuator locations (mm)

i	x_0	y_0
1	299.40	250.82
2	450.21	250.82
3	450.21	125.41
4	100.96	123.82
5	434.34	346.07

Table 3.2: Sensor locations (mm)

i	x_0	y_0
1	133.35	64.77
2	133.35	214.78
3	133.35	316.23
4	133.35	413.00
5	253.20	64.77
6	253.20	214.78
7	253.20	316.23
8	253.20	413.00
9	373.06	64.77
10	373.06	214.78
11	373.06	316.23
12	373.06	413.00
13	485.70	64.77
14	485.70	214.78
15	485.70	316.23
16	485.70	413.00

and we can consider each piezoelectric to act electrically independent. That is, the charge/voltage combination on a given piezoelectric is a direct function of the modal position only and not of charge/voltage combinations on other piezoelectrics. This might not necessarily be the case for a complicated electrode arrangement where electrodes on the top and bottom of a piezoelectric may overlap.

At this point expressions for the control system electronics can be included. The electronics couples dynamically through the piezoelectric voltage and charge, v and q. Hagood et al. (1990) discuss, in general terms, how to incorporate electronics into a state-space representation of the piezosystem. Much effort was used in the design of the MIMO plate control testbed to insure that the sensor and actuator electronics would be simple to model and integrate well with the piezostructure.

Chapter 4

Piezo-Electronics Design

Investigations into piezoelectrics as both sensor and actuators have been pursued because of the reasonably simple electromechanical coupling between a structure and the electronics associated with passive and active controllers. Hagood et al. (1989 1990) discuss modelling of piezoelectric systems coupled with electronics. This coupling could be incorporated in active and/or passive control schemes. Passive electronics can modify the dynamics of the mechanical system through the electromechanical coupling offered by the piezoelectrics and have been used to add passive damping to a structure. This chapter is concerned with methods for regulating voltage-driven actuators and measuring sensor voltage correlated to modal positions.

4.1 Actuator Amplifiers and Smoothing Filters

The actuator equation (3.16) shows that, for voltage-driven actuators, the force input is proportional to the patch voltage and that the current does not influence modal forces. Current will flow to or from a patch depending upon the modal velocities. The flow of current either with or against the forcing voltage is analogous to deflections either with or against a point force resulting in energy flow to or from the structure.

Piezoelectric actuators typically require large voltages and relatively small cur-

rents. Several techniques for providing a control voltage were considered, among them: High voltage analog amplifiers, pulse width modulated amplifiers. Due primarily to the high cost high voltage amplifers were eliminated. It was unknown how pulse width modulated amplifiers would affect a piezostructure and were also disregarded. The voltage amplification scheme chosen for the MIMO test bed is a power amplifier in series with an audio transformer (see figure 4.1). Audio transformers were chosen since they have flat frequency responses over a large bandwidth (2–20,000 Hz). The power amplifier is needed since most D/A boards do not provide sufficient power. The transformer steps up the control voltage as necessary. Admittedly, the current on the patch side of the transformer is low but this is satisfactory since piezoelectrics are low power actuators. The fact that the transformers do not transfer DC voltages is of little concern since we are dealing with harmonic and narrowband sinusoidal disturbances.

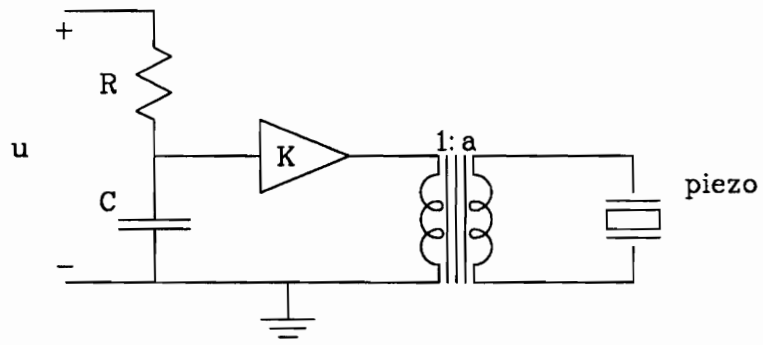

Figure 4.1: Filter–Amplifier–Transformer Diagram

The effective amplifier gain is the voltage amplifier gain multiplied by the turns

ratio of the transformer.

$$V_{out} = aKV_{in} \tag{4.1}$$

The transformer selected has a turns ratio $a \simeq 24 : 1$ and the voltage amplifier has a gain of $K \simeq 2.5V/V$.

To reduce the effect of the staircased nature of the control signal output from the D/A board on higher modes of the plate, the control signal is filtered using a single pole passive low pass filter (see figure 4.1) with transfer function

$$\frac{V_{out}}{V_{in}} = \frac{1}{sRC + 1} \tag{4.2}$$

The smoothing filter pole was selected at 200 Hz. At present, the controller software runs at approximately 2000 Hz, allowing control of strucutral frequencies one decade below, at 200 Hz. The smoothing filter sufficiently attenuates the high frequency components of the staircased control signal.

Burst random testing of the smoothing filter–amplifier–transformer combination was performed. A curve fit of the data resulted in a transfer function

$$\frac{V_{out}}{V_{in}} = 0.514\frac{(s/18.9 + 1)}{(s/38 + 1)(s/1260 + 1)} \tag{4.3}$$

Figure 4.2 shows the curve fit versus the measured data.

4.2 Sensor Design

It is possible to impose appropriate boundary conditions to piezoelectric sensors such that the voltage is a linear transformation of modal positions. This can be achieved by imposing an open circuit across the sensor patch electrodes. This forces the current, thus the charge, flowing from a patch to be zero. Using this boundary condition the sensor equation (3.17) becomes,

$$v_i = -C_p^{-1}\Theta_i^T r \tag{4.4}$$

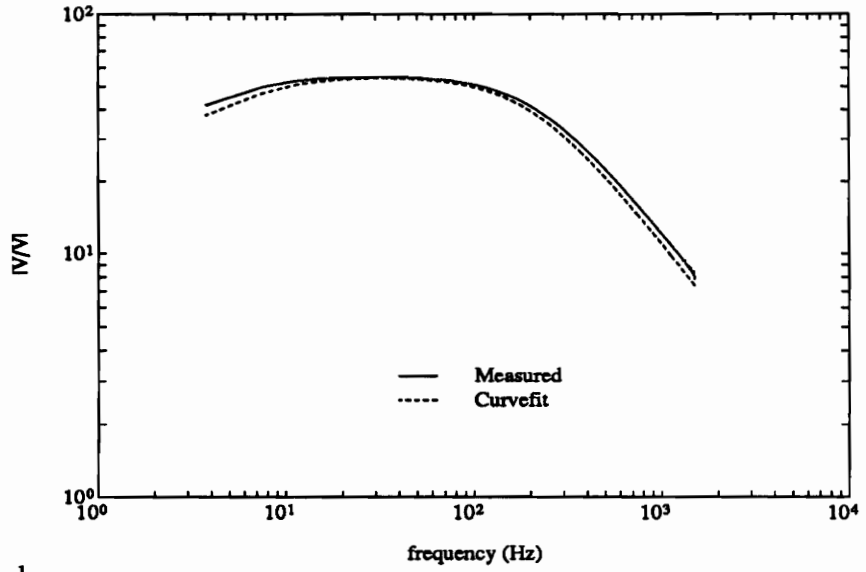

a. magnitude

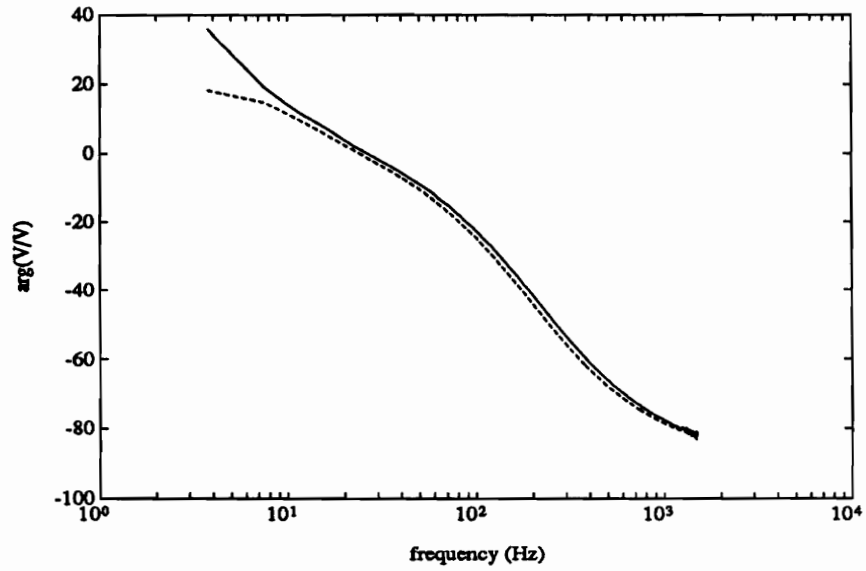

b. phase

Figure 4.2: Curvefit and Experimental FRF's for Filter-Amplifier-Transformers

In a practical sense it is difficult to impose real open circuits and still be able to measure the voltage of interest. Large impedances placed across electrodes can cause impedance mismatches with voltage measuring equipment and load the piezoelectric changing the quantity to be measured. Also conventional A/D boards do not measure the typically small voltages output by PVDF which fill only a few bits of information on the A/D board. Therefore it is desirable to amplify the signal.

Imposing the boundary condition and amplifying is possible using operational amplifiers (op-amps) by connecting the piezoelectric to a non-inverting amplifier (see figure 4.3). The infinite input impedance and zero input bias current of ideal op-amps satisfies the open circuit boundary condition. In reality op-amps have finite input impedance and allow current to flow into the inputs of the op-amp. It is necessary to choose an op-amp with sufficiently large input impedance such that the cutoff frequency ($1/2\pi RC_p$) for the resulting high-pass filter is as low as required. The gain of the non-inverting amplifier is selected as needed.

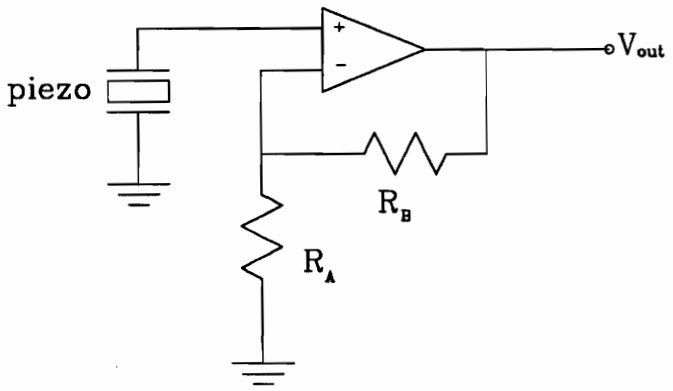

Figure 4.3: Noninverting Amplifier Schematic

The PVDF sensors used on the plate test bed have small capacitances (2.5 pF) with correspondingly large impedances over the frequency range of interest (40–250 Hz). This required the use of high input impedance JFET op-amps (Burr Brown OPA 602) to keep the cutoff frequency sufficiently low. Also the low bias currents provided by junction field-effect transistor (JFET) op-amps are a benefit. The non-inverting amplifier was designed to have a gain of 11 V/V.

Experimentation showed that a low pass filter would also be required to eliminate high frequency noise. A single pole active low-pass filter was designed to have a cutoff at 40 kHz. The sensitivity of the PVDF sensors to very low frequency vibration necessitated the use of a high-pass filter in the signal conditioning amp. This was added as a second stage and follows a Sallen-Key design, see figure 4.4. The second stage was designed with a gain of 1.8 V/V, making the overall amplifier gain 20 V/V. The final sensor signal conditioning amplifier design is shown in figure 4.5. A frequency response of a sensor signal conditioning amplifier is shown in figure 4.6. The spikes in the frequency response of the signal conditioning amplifier are a result of noise at 60 Hz harmonics.

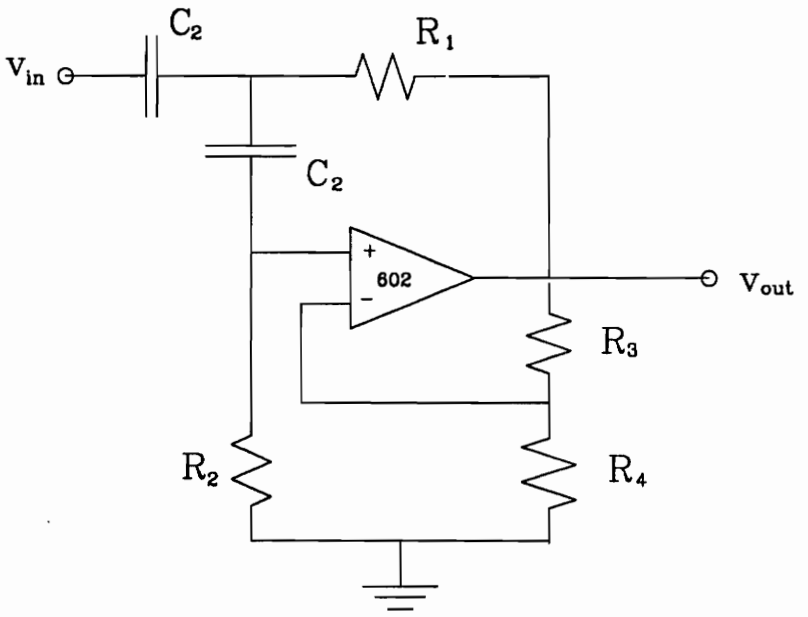

Figure 4.4: Sallen-Key High Pass Filter Schematic

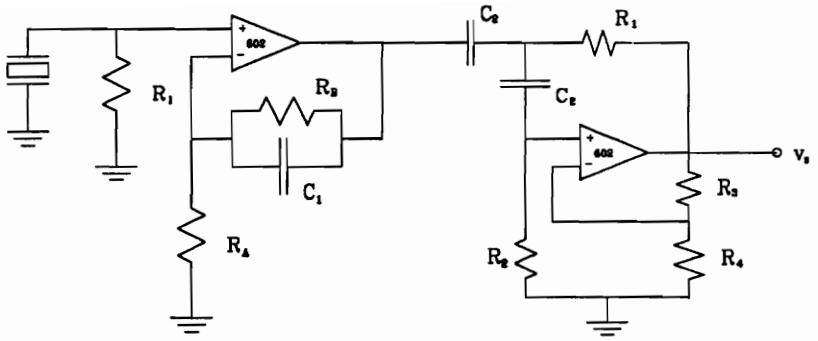

Figure 4.5: Signal Conditioning Amplifier Schematic

Table 4.1: Signal Conditioning Amplifier Component Values

R_A	1.00	kΩ
R_B	10.00	kΩ
R_I	22.00	MΩ (1–8)
	10.00	MΩ (9–16)
C_1	0.41	nF
C_2	0.57	μF
R_1	100.00	kΩ
R_2	100.00	kΩ
R_3	220.00	kΩ
R_4	390.00	kΩ

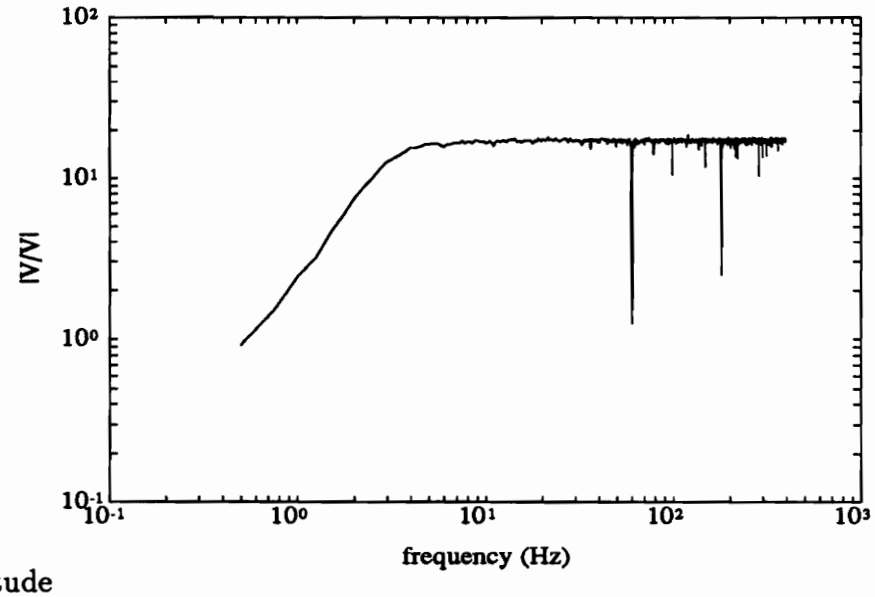

a. magnitude

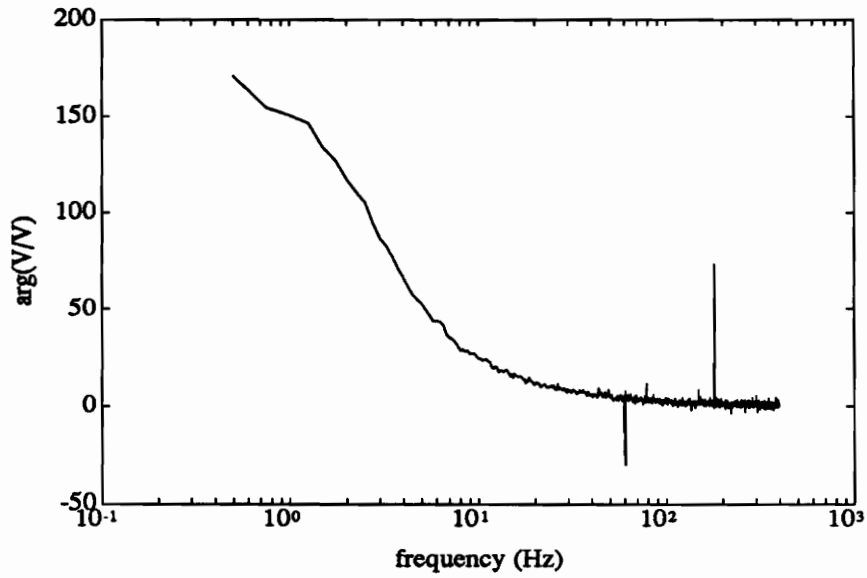

b. phase

Figure 4.6: FRF for Sensor Signal Conditioning Amp, Channel 5

Chapter 5

System Identification

Essential to the success of modern feedback control methods is an accurate mathematical description of the system to be controlled. Research conducted to date has relied on reasonably accurate analytical models to describe physical systems. This approach is insufficient when dealing with more complicated structures found outside the laboratory. The author has found no research conducted which provides a method to determine piezoelectric system parameters, such as Θ, experimentally. This chapter describes system identification methods which can be used to determine models of piezostructures experimentally. Initial system identification results for the MIMO plate control test bed are also shown.

5.1 Model Generation Method

Considering the piezostructure as a MDOF system with the sensor outputs a linear combination of the generalized coordinates r, the system can be described as follows,

$$M\ddot{r} + C\dot{r} + Kr = \Theta v \tag{5.1}$$

$$v = -C_p^{-1}\Theta^T r \tag{5.2}$$

At this point the generalized coordinate, r, can be considered to be arbitrary.

Performing a change of basis into a modal domain changes the system representation to

$$\ddot{q} + \{2\zeta_r\omega_r\}\dot{q} + \{\omega_r^2\}q = \Phi^T\Theta v \tag{5.3}$$

$$v = -C_p^{-1}\Theta^T\Phi q \tag{5.4}$$

where the generalized coordinate r is a linear combination of the modal coordinates q.

$$r = \Phi q \tag{5.5}$$

The eigenvector matrix Φ is mass normalized such that $\Phi^T M\Phi = I$. The matrices $\{2\zeta_r\omega_r\}$ and $\{\omega_r^2\}$ are diagonal and represent damping and natural frequencies for the r^{th} mode.

So far it has not been necessary to know the parametric matrices that describe the piezosystem. The above modal equations are similar to those developed for a point force response. The quantity which is as yet undetermined is the electromechanical coupling matrix, Θ.

Using the modal sensor equation the i^{th} sensor voltage as a function of the j^{th} actuator can be represented as,

$$V_{s,i} = -C_p^{-1}{}_{s,i}\sum_{r=1}^{N}\theta_{s,i}^r\phi_{s,i}^r q_j^r \tag{5.6}$$

and from the modal actuator equation

$$q_j^r = \frac{\phi_{a,j}^r\theta_{a,j}^r V_{a,j}}{(\omega_r^2 - \omega^2) + j(2\zeta_r\omega\omega_r)} \tag{5.7}$$

Combining equations 5.6 and 5.7 gives

$$V_{s,i} = -C_p^{-1}{}_{s,i}\sum_{r=1}^{N}\frac{\theta_{s,i}^r\phi_{s,i}^r\phi_{a,j}^r\theta_{a,j}^r}{(\omega_r^2 - \omega^2) + j(2\zeta_r\omega\omega_r)}V_{a,j} \tag{5.8}$$

Let

$$\hat{\theta}_i^r = \theta_i^r\phi_i^r \tag{5.9}$$

which is, in reality, the electromechanical coupling matrix in the new modal basis. Now we can represent equation 5.8 in a pole residue model,

$$\frac{V_{s,i}}{V_{a,j}} = -C_p^{-1}{}_{s,i} \sum_{r=1}^{N} \left[\frac{A_{ij}^r}{(s-p_r)} + \frac{A_{ij}^{r\,*}}{(s-p_r^*)} \right] \tag{5.10}$$

where

$$A_{ij}^r = \frac{\hat{\theta}_{s,i}^r \hat{\theta}_{a,i}^r}{j2\omega_r\sqrt{1-\zeta_r^2}} \tag{5.11}$$

$$p_r = -\zeta_r\omega_r + j\omega_r\sqrt{1-\zeta_r^2} \tag{5.12}$$

Now curve fitting algorithms can be used to estimate values of ω_r, ζ_r and $\hat{\theta}_i^r$ and use them to form a modal state space model. It is assumed that the capacitance of the sensor, C_p, is known.

5.2 Initial Testbed System Identification Results

The transputer based D/A system was used to acquire data from the plate sensors. The 17 frequency response functions (includes a drive point), calculated by the 12-channel analyser TFAS12. TFAS12 is a custom frequency analyser, writen in C, that utilizes the T800 Transputer microprocessor to provide 12 simultaneous frequency response functions. The frequency response functions were then uploaded to the VAX for the curve fitting routine MODHAN. This routine provides estimates for the poles and residues of the system, using a viscous damping model.

The calculated data was then down-loaded to a personal computer for calculation of the electromechanical coupling coefficients. Of primary importance is the drive point. Since the sensors were constructed with PVDF and the actuators with PZT the electromechanical coupling coefficients $\hat{\theta}_i^r$ are different.

$$\theta_i^r = e_{31,i} S_i \int\int \left(\frac{\partial^2 \Psi_r}{\partial x^2} + \frac{\partial^2 \Psi_r}{\partial y^2} \right) dy dx \tag{5.13}$$

The difference between the actuators and sensors is the product $e_{31}S_i$. This is because the materials have different electromechanical properties and are of different thickness. The evaluation of the integral does not change for the drive point since both actuator and sensor act over the same strain field. It was assumed for the PVDF that the field-stress constant e is the same in the 1 and 2 directions. This is not true and in fact they differ by about a factor of 2, and an average value was used in the analysis. This assumption does not appear to affect the results.

The product $e_{31}S_i$ was factored out of the residuals and the eigenvectors were found. Then the quantity was multiplied back in to yield estimates for $\hat{\Theta}$. Figures 5.1 and 5.2 compare measured FRF's with those found using the curve fit, and an analytical model. As expected, the curvefit matches zeros in the structure much better than the analytical model. This is important since the position of the zeros is directly affected by the electromechanical coupling coefficients. The model developed from the system ID can now be used in the design of a controller.

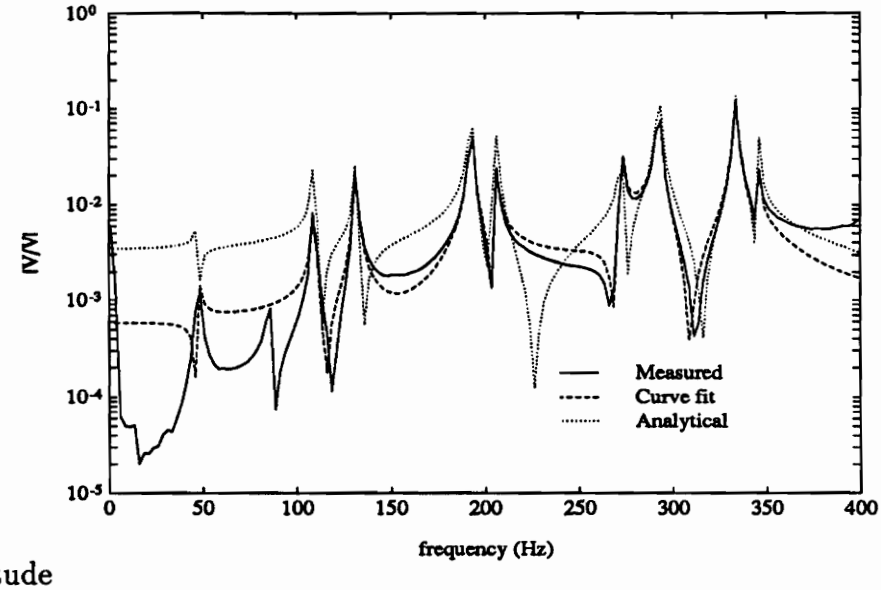

a. magnitude

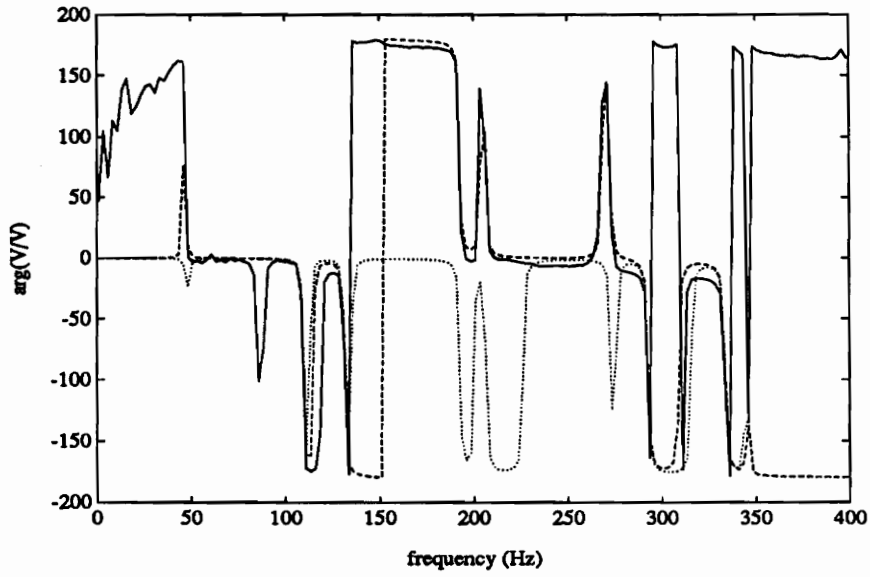

b. phase

Figure 5.1: Curvefit and Experimental FRF's for Sensor # 1

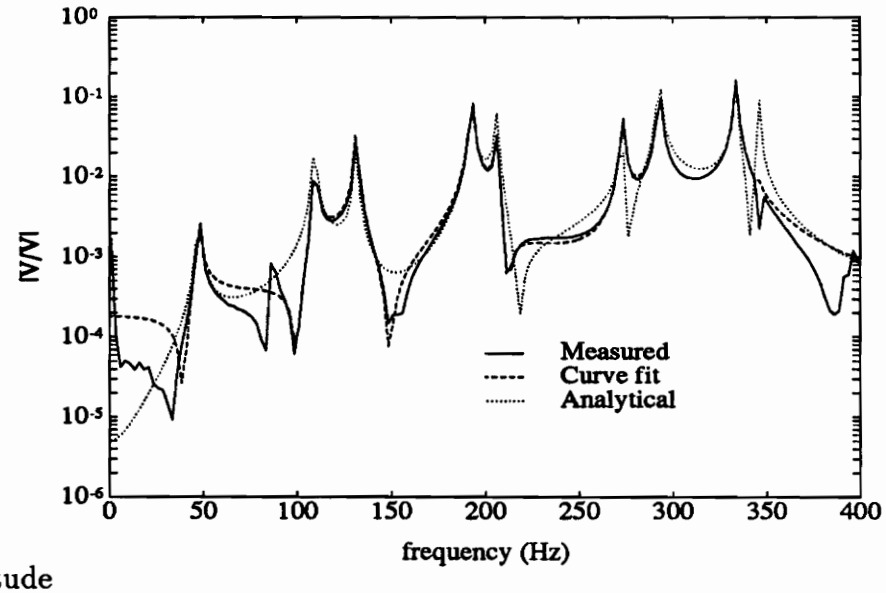

a. magnitude

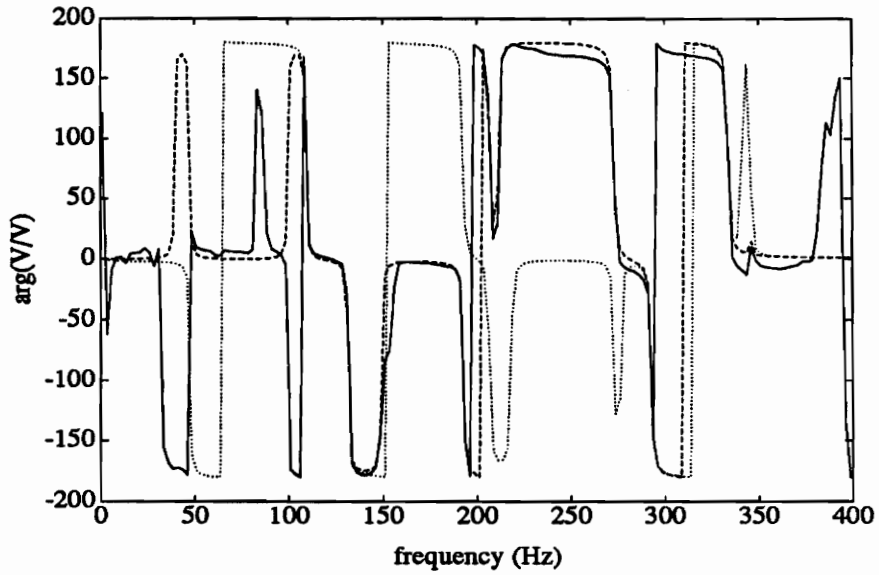

b. phase

Figure 5.2: Curvefit and Experimental FRF's for Sensor # 13

Chapter 6

SIMO LQG Control

The empirical model developed in chapter 5 was used in initial SIMO control experiments to demonstrate the testbed closed-loop performance. A Linear Quadratic Gaussian (LQG) controller, which combines Linear Quadratic Regulator feedback control with an optimal stochastic estimator (Kalman filter), was used. This feedback controller minimizes a quadratic cost functional which weighs system states against controller effort (Rubenstein 1991).

Using a discrete representation of the augmented state equations described in chapter 4 a LQR feedback control law was computed using MATLAB's DLQR function. The feedback control law is of the form

$$u_k = -K\hat{x}_k \tag{6.1}$$

The Kalman filter gains were calculated using MATLAB's DLQE function which yields an estimator of the form

$$\hat{x}_{k,k-1} = \Phi\hat{x}_{k-1,k-1} + \Gamma u_{k-1} \tag{6.2}$$

$$\hat{y}_k = C\hat{x}_{k,k-1} \tag{6.3}$$

$$\hat{x}_{k,k} = \hat{x}_{k,k-1} + K_f(y_k - \hat{y}_k) \tag{6.4}$$

Rubenstein (1991) discusses in greater detail the formation of continuous and discrete

system representations, the development of discrete time controllers, and the analysis of discrete compensators for transient control and disturbance rejection.

The SIMO control experiment studied vibration control of the testbed using Actuator #4 and all sixteen piezoelectric sensors. A 110 Hz, 1 volt harmonic disturbance was applied to Actuator #5. The simulated and experimental responses for modes 1 and 2 are shown in figures 6.1 and 6.2. Experimental results for modes 3, 4 and 5 as well as the control voltage are shown in figures 6.3–6.6. The active vibration control results in multi-mode suppression, with approximately 6 dB reduction in mode 2, whose resonant frequency is close to the excitation frequency.

The discrepancies between the simulation and the experiment indicates the need for a better system identification. Better eigenvectors and electromechanical coupling coefficients would produce improved estimates of modal states. This would directly affect the closed-loop response of the system not only in the SIMO control scheme discussed here, but also in MIMO control work done in the future.

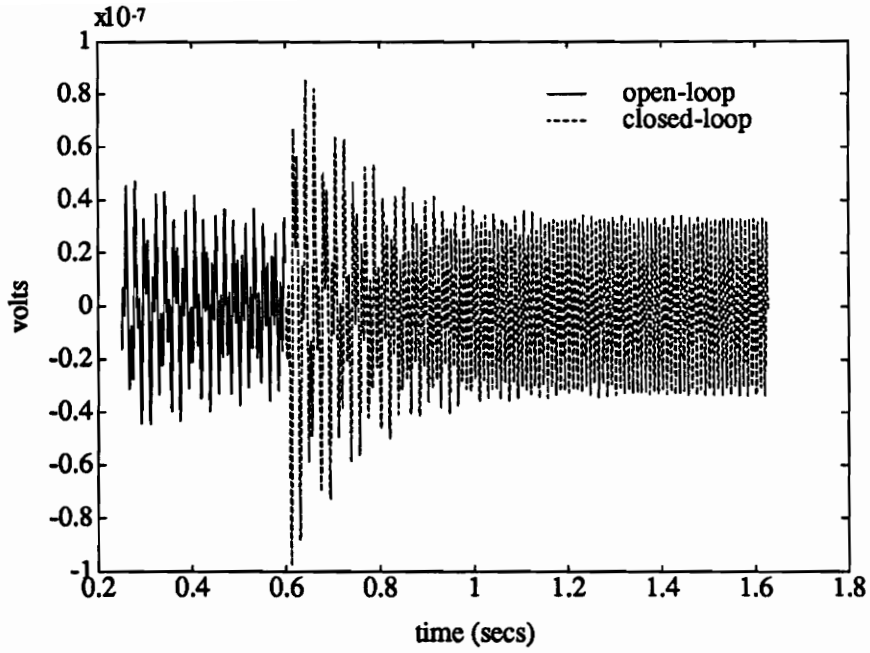

a. simulation

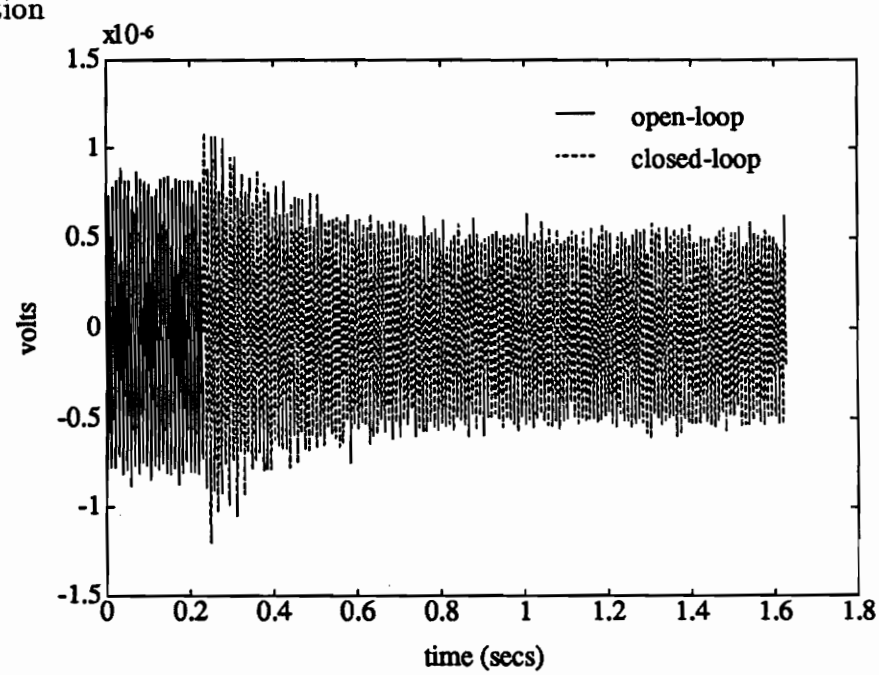

b. experiment

Figure 6.1: MIMO Plate Control: Experiment and Simulation for 110 Hz Disturbance, Mode 1

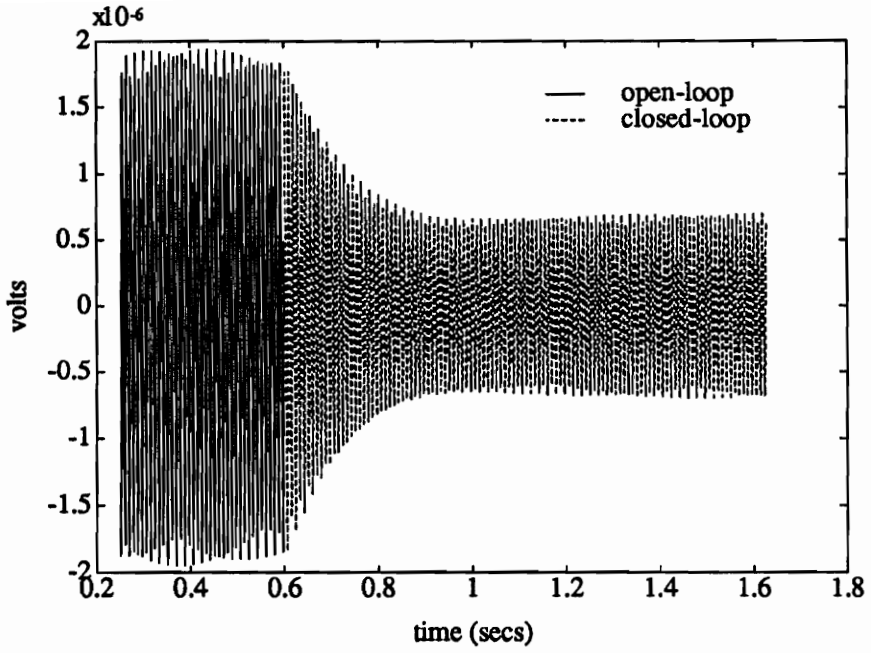

a. simulation

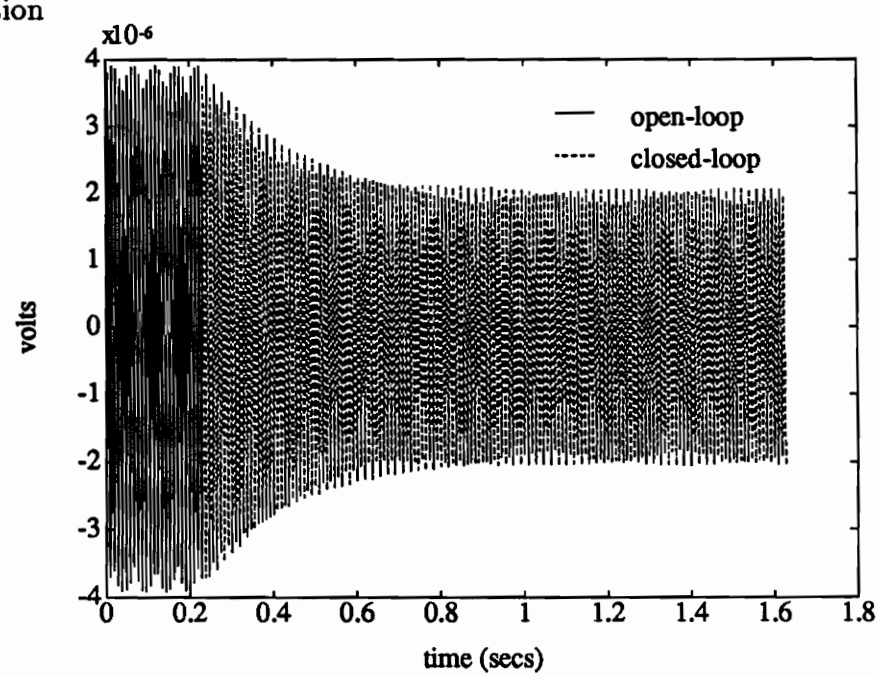

b. experiment

Figure 6.2: MIMO Plate Control: Experiment and Simulation for 110 Hz Disturbance, Mode 2

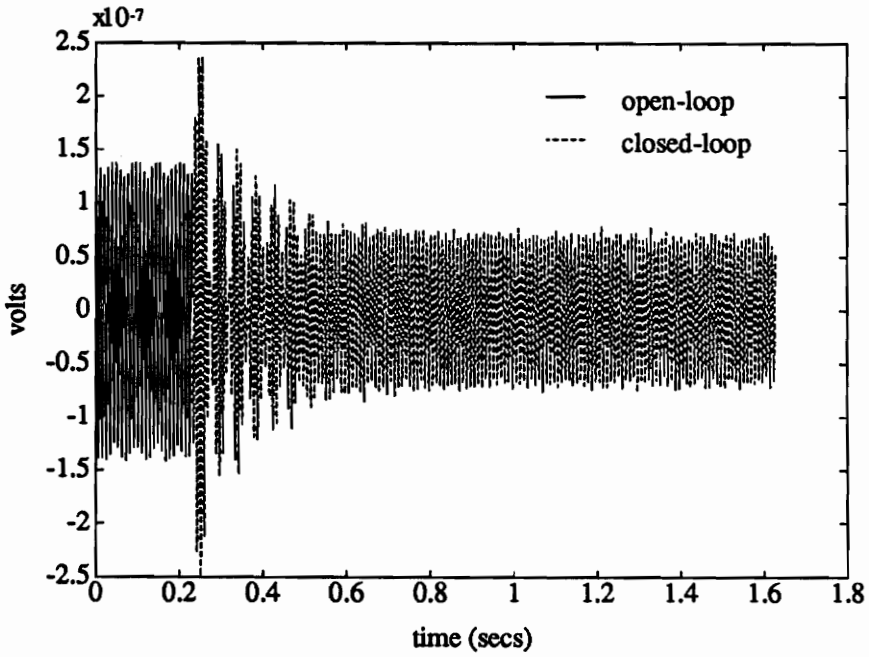

Figure 6.3: MIMO Plate Control Experiment for 110 Hz Disturbance, Mode 3

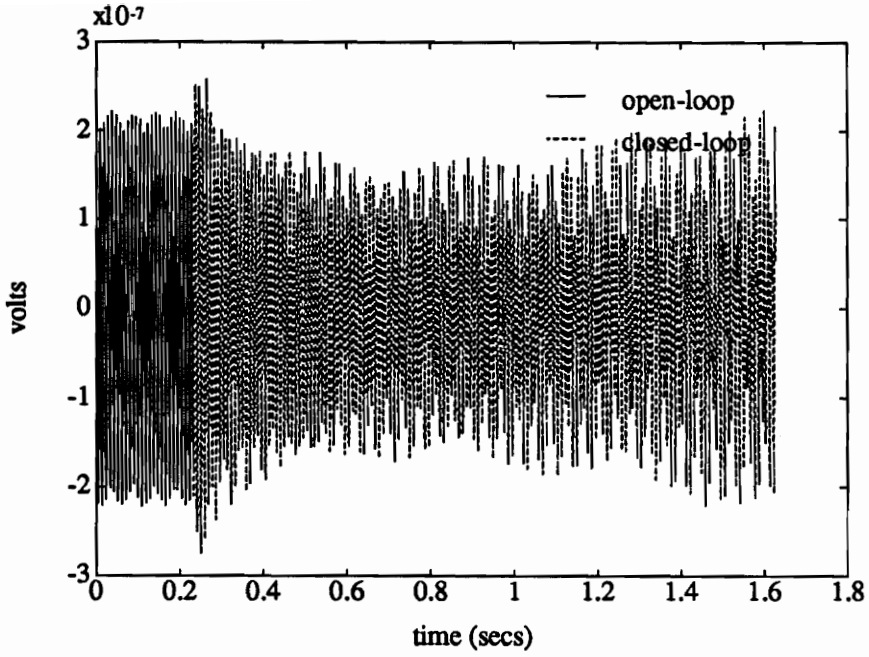

Figure 6.4: MIMO Plate Control Experiment for 110 Hz Disturbance, Mode 4

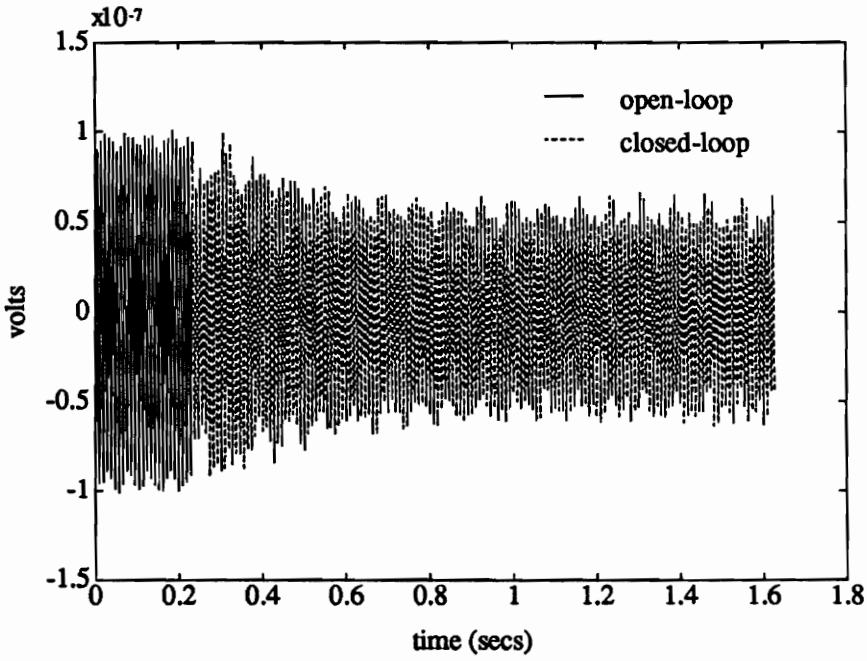

Figure 6.5: MIMO Plate Control Experiment for 110 Hz Disturbance, Mode 5

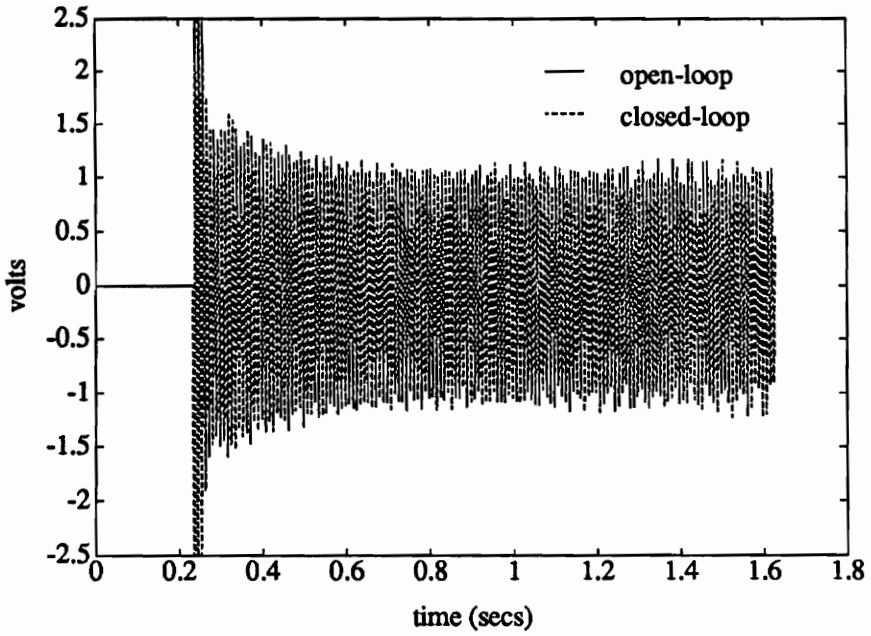

Figure 6.6: MIMO Plate Control Experiment for 110 Hz Disturbance, Control Signal

Chapter 7

Summary

This work discusses the design and development of a MIMO plate control testbed. This testbed will be utilized as a development site and a standard comparison site for Active Vibration Control and Active Structural Acoustic Control. The testbed constructed is an extension of a SIMO plate control testbed developed in the Smart Structures Lab at VPI&SU (Rubenstein 1991). While the SIMO plate used proven technology in shakers and accelerometers, the new MIMO testbed implements piezotechnology, taking advantage of piezoelectrics' compact size and weight.

An analytical model which represents the electromechanical interaction between the structure, piezoelectrics and electronics is developed (Hagood 1990) and used in the design of amplifiers for both piezoactuators and piezosensor signals. This model is also used in an initial approach to an effective piezosystem identification.

A single pole passive smoothing filter was used to reduce the effect of the zero-order-held control signal. The smoothing filter was used in conjunction with a voltage amplifier and transformer to provide the relatively high voltages required by piezoelectric actuators. Measured dynamics of the filter-amplifier-transformer (FAT) combinations was curvefit and the resulting transfer function was used in the design of control laws for the plate. While the FAT's are simple to build, low frequency dynam-

ics should be modeled. The low frequency pole and zero are thought to represent the transformer dynamics. Other amplification schemes, such as pulse width modulation, may only require modeling of designed smoothing filter and could draw less power, both benefits which may be necessary in large scale applications of this technology.

Sixteen PVDF sensors were conditioned to measure plate position. This required the design of high impedance signal conditioning amplifiers. It is also possible to measure plate velocities using current-to-voltage (I-V) amplifiers. The PVDF sensors used on the MIMO plate deliver small currents (less than 1 μA) which requires high gain I-V amplifiers which may be more subject to various sources of noise.

PZT sensors deliver $\sim$25 times the voltage and $\sim$250 times the current as PVDF sensors of similar area. Both of these properties indicate that PZT is a better transducer than PVDF. Recent studies have investigated the used of piezoelectric sensoriactuators which use a single piezoelectric element to provide measurement and control. There are also indications that sensoriactuators could be used effectively in system identification schemes to provide drive point responses.

The initial results in the system identification of the MIMO plate testbed provided electromechanical coupling coefficients used in the state space representation of the system. The model was used in initial experiments and simulations of SIMO control of the plate. The results of the closed-loop control experiments and simulation indicate that a better identification of the plate is required to achieve improved closed-loop estimation and response. In addition, a better system ID is necessary to design and build MIMO controllers.

The MIMO plate control testbed will be used to investigate not only other actuator and sensor materials and architechtures, but also differenct control approaches and improved computational hardware. Control approaches include: reduced order

control, robust control, on-line adaptive control, advanced hybrid techniques, and hierarchical control.

References

- Bailey, Thomas and James E. Hubbard, Jr. 1985. "Distributed Piezoelectric-polymer Active Vibration Control of a Cantilever Beam", *Journal of Guidance and Control* 8(5), pp. 605–611.

- Baz, A. and S. Poh. 1987. "Optimum Vibration Control of Flexible Beams by Piezo-electric Actuators", NASA-CR-180209; N87-18880.

- —. 1988. "Performance of an Active Control System with Piezoelectric Actuators", *Journal of Sound and Vibration* 126(2), pp. 327–343.

- —. 1990. "Experimental Implementation of the Modified Independent Modal Space Control Method", *Journal of Sound and Vibration* 139(1), pp. 133–149.

- Burke, Shawn E. and James E. Hubbard, Jr. 1991. "Distributed Transducer Vibration Control of Thin Plates", *Journal of the Acoustical Society of America* 90(2), Pt. 1, pp. 937–944.

- Chiang, Wen-Wei and Chih-Kung Lee. 1989. "Critical Active Damping Control of a Flexible Slender Plate Using a Distributed Modal Actuator Sensor", Presented in 1989 American Control Conference, Pittsburgh, PA, pp 700–705.

- Clark, Robert L. and C. R. Fuller. 1991. "Control of Sound Radiation with Adaptive Structures", *J. of Intelligent Materials Systems and Structures* Vol 2.

pp. 431–452.

- —. 1990. "Experiments on Active Control of Structurally Radiated Sound Using Multiple Piezoceramic Actuators"

- Clark, Robert L., Chris R. Fuller and Al Wicks. 1991. "Characterization of Multiple Piezoelectric Actuators for Structural Excitation", *Journal of the Acoustical Society of America*, 90(1), pp. 346–357.

- Crandal, Stephen H., Dean C. Karnopp, Edward F. Kurtz, Jr., and David C. Pridmore-Brown. 1968. *Dynamics of Mechanical and Electromechanical Systems*, Robert E. Krieger Publishing Co., Malabar, FL.

- Crawley, Edward F. and Eric H. Anderson. 1989. "Detailed Models of Piezoceramic Actuation of Beams", AIAA 89-1388-CP.

- Crawley, E. F. and K. B. Lazarus. 1989. "Induced Strain Actuation of Isotropic and Anisotropic Plates", AIAA 89-1326-CP.

- Crawley, Edward F. and Javier de Luis. 1987. "Use of Piezoelectric Actuators as Elements of Intelligent Structures", AIAA Journal, vol. 25, no. 10, pp 1373–1385.

- Cudney, H. H., 1989. "Distributed Structural Control Using Multilayered Piezoelectric Actuators", Ph.D. Dissertation, State University of New York at Buffalo, September.

- de Luis, Javier and Edward F. Crawley. 1990. "Experimental Results of Active Control on a Prototype Intelligent Structure", AIAA 90-1163-CP.

- Dimitriadis, E. K., C. R. Fuller and C. A. Rogers. 1991. "Piezoelectric Actuators for Distributed Vibration Excitation of Thin Plates", *Journal of Vibration and Acoustics* Vol. 113, pp. 100–107.

- Flemming, Mark Richard. 1990. "An Experimental Investigation of the Harmonic Excitation of Simply Supported Plate with Surface-Bonded Piezoceramic Actuators", Master's Thesis, VPI&SU.

- Gibbs, Gary P. and Chris R. Fuller. 1990. "Experiments on Active Control of Vibrational Power Flow Using Piezoceramic Actuators and Sensors", AIAA 90-1132.

- Hagood, Nesbitt W. and Edward F. Crawley. 1989. "Experimental Investigation into Passive Damping Enhancement for Space Structures", AIAA 89-3436-CP.

- Hagood, Nesbitt W. and Andreas von Flotow. 1989. "Damping of Structural Vibrations with Piezoelectric Materials and Passive Electrical Networks", *Proceedings of Damping '89*, West Palm Beach, FL. pp. ICC-1–ICC-31.

- Hagood, Nesbitt W., Walter H. Chung, Andreas von Flotow. 1990. "Modelling of Piezoelectric Actuator Dynamics for Active Structural Control", AIAA-90-1087-CP.

- Hanagud, S., M. W. Obal and A. J. Calise. 1987. "Optimal Vibration Control by the Use of Piezoceramic Sensors and Actuators", AIAA 87-0959.

- Hanagud, S., C. C. Won and M. W. Obal. 1988. "Optimal Placement of Piezoceramic Sensors and Actuators", *Proceedings of American Controls Conference*, Atlanta, GA, Vol 3., pp 1884–1889.

- Im, Seyoung and S. N. Atluri. 1989. "Effects of a Piezo-Actuator on a Finitely Deformed Beam Subjected to General Loading", *AIAA Journal*, 27(12), pp 1801–1807.

- Lee, C.-K., W.-W. Chiang and T. C. O'Sullivan. 1989. "Piezoelectric Modal Sensors and Actuators Achieving Critical Active Damping on a Cantilever Plate", AIAA 89-1390-CP.

- —. 1991. "Piezoelectric Modal Sensor/Actuator Pairs for Critical Active Damping Vibration Control", *Journal of the Acoustical Society of America*, 90(1), pp.374–384.

- Lee, C.-K. and T. C. O'Sullivan. 1991. "Piezoelectric Strain Rate Gages", *Journal of the Acoustical Society of America* 90(2) pt. 1, pp 945–953.

- Mason, Warren P. 1981. "Piezoelectricity, Its History and Applications", Journal of the Acoustical Society of America 70(6), pp. 1561–1566.

- Moerder, Daniel D. and Anthony J Calise. 1985. " Convergence of a Numerical Algorithm for Calculating Optimal Output Feedback Gains", *IEEE Transactions on Automatic Control*, Vol. AC-30, No. 9.

- Pan, Jie, Colin H. Hansen and Scott D. Snyder. 1991. "A Study of the Response of a Simply Supported Beam to Excitation by a Piezoelectric Actuator", *Proceedings of the Conference on Recent Advances in Active Control of Sound and Vibration*, pp. 39–49.

- Rubenstein, Stephen P. 1991. "An Experiment in State-Space Vibration Control of Steady Disturbances on a Simply-Supported Plate", Master's Thesis, VPI&SU.

- Sung, Chia-Chi, Vasundra V. Varadan, Xiao-Qi Bao, and Vijay K. Varadan. 1990. "Active Control of Torsional Vibration Using Piezoceramic Sensors and Actuators", AIAA 90-1130-CP.

- Swigert, Charles J. and Forward, Robert L. 1981. "Electronic Damping of Orthogonal Bending Modes in a Cylindrical Mast – Theory & Experiment", *J. Spacecraft* 18(1), pp 5–17.

- Tzou, H. S. 1992. "A New Distributed Sensor and Actuator Theory for 'Intelligent' Shells", *Journal of Sound and Vibration* 153(2), pp 335–349.

- Tzou, H. S. and M. Gadre. 1989. "Theoretical Analysis of a Multi-layered Thin Shell Coupled with Piezoelectric Shell Actuators for Distributed Vibration Controls", *Journal of Sound and Vibration* 123(3), pp.433–450.

- Tzou, H. S. and C. I. Tseng. 1990a. "Distributed Piezoelectric Sensor/Actuator Design for Dynamic Measurement/Control of Distributed Parameter Systems: A Piezoelectric Finite Element Approach", *Journal of Sound and Vibration*, 138(1), pp 17–34.

- —. 1990b. "Distributed Dynamic Identification and Controls of Flexible Shells", AIAA-90-1089-CP.

- Wang, Bor-Tsuen and Craig A. Rogers. 1990 "Laminate Plate Theory for Spatially Distributed Induced Strain Actuators", *Proceedings of the Fifth Japan-U.S. Conference on Composite Materials*, Tama City, Japan.

- —. 1991. "Modelling of Finite-Length Spatially-Distributed Induced Strain Actuators for Laminate Beams and Plates", AIAA-91-1258-CP.

Vita

Daniel G. Cole was born in Roanoke, Virginia on September 13, 1968. He grew up in Roanoke and graduated from North Cross School in 1986. Having known he wanted to be an engineer since childhood (and being born into the profession) he went to Virginia Tech and received a Bachelor of Science Summa Cum Laude in Mechanical Engineering in 1991. As an undergraduate he worked in the Cooperative Education program with both the U. S. Navy at David Taylor Research Center (boring) and Babcock & Wilcox SPIS (long hours). His labor as a co-op convinced him that he does not want to look things up in catalogs for a living, so he decided to continue his education in graduate school at Virginia Tech. After receiving his Master of Science in Mechanical Engineering in September 1992, he will continue working at Virginia Tech as a Cunningham Fellow in pursuit of a Doctor of Philosophy.